Surface modification of monocrystalline zinc oxide induced by high-density electronic excitation

Luc Museur, Alexandra Manousaki, Demetrios Anglos, and Andrei V. Kanaev

Citation: J. Appl. Phys. **110**, 124310 (2011); doi: 10.1063/1.3671006
View online: http://dx.doi.org/10.1063/1.3671006
View Table of Contents: http://jap.aip.org/resource/1/JAPIAU/v110/i12
Published by the American Institute of Physics.

Surface modification of monocrystalline zinc oxide induced by high-density electronic excitation

Luc Museur,[1] Alexandra Manousaki,[2] Demetrios Anglos,[2,3] and Andrei V. Kanaev[4,a)]
[1]*Laboratoire de Physique des Lasers, LPL CNRS, Institut Galilée, Université Paris 13, 93430, Villetaneuse, France*
[2]*Institute of Electronic Structure and Laser, Foundation for Research and Technology–Hellas (IESL-FORTH), P.O. Box 1385, GR-71110 Heraklion, Crete, Greece*
[3]*Department of Chemistry, University of Crete, P.O. Box 2208, GR-71003 Heraklion, Crete, Greece*
[4]*Laboratoire des Sciences des Procédés et des Matériaux, LSPM CNRS, Institut Galilée, Université Paris 13, 93430 Villetaneuse, France*

(Received 30 June 2011; accepted 16 November 2011; published online 20 December 2011)

Strong modifications of semiconductors can be provoked by high-density electronic excitation. We report on surface structuring of monocrystalline wurtzite O-face (0001) ZnO excited by UV femtosecond laser pulses (248 nm) below the ablation threshold. At fluences above 11 mJ/cm^2, nanoholes of D=10 nm diameter appear quasi-periodically separated by a distance ~30 nm (=3 D). Dual-pulse (pump-pump) experiments permit estimation of the electronic excitation lifetime responsible for this nanostructuring, which is in agreement with the electron-hole plasma lifetime 220 ps. The nanostructuring results in a smaller monocrystalline domain of ~0.1 μm size and increases the crystalline interplane c-distance by 0.11%. The excitonic luminescence of the irradiated sample is found to increase by about 10 times. The nanostructuring remains stable in a limited range of laser fluences: above 40 mJ/cm^2 the surface melts, which accelerates the photoinduced bonds breaking leading to surface erosion. We tentatively ascribe the related mechanism to the nucleation-growth of cluster vacancies at crystal dislocations accelerated by the non-thermal (electronic) melting of the surface layer. At fluences lower than 11 mJ/cm^2, larger volcano-like features of 60-nm diameter were observed. The characteristic crater shape and irregular surface repartition permit their assignment to thermal explosion of impurities due to multiple exciton condensation. © *2011 American Institute of Physics*. [doi:10.1063/1.3671006]

I. INTRODUCTION

Optical excitation of semiconductor crystals at or near their bandgap by use of low-intensity radiation (low-I) has been shown to produce macroscopic mechanical modifications on the crystal surface. This type of effect is often called single-photon damage or etching and is principally related to the breaking of chemical bonds, following photoexcitation into anti-bonding states, and the formation of single and cluster vacancies that in turn lead to lattice instabilities, which eventually manifest themselves as macroscopic surface modifications.[1,2] The anti-bonding states can be reached even when the incident photon energy is not sufficient for direct excitation, via the so-called two-hole surface states, whose formation competes with the relaxation process taking place on the sub-nanosecond time scale. In fact, transition to the anti-bonding state can be achieved by successive excitation events. Finally, in this low-I irradiation regime, desorption of excited products may also appear as a result of the negative electron affinity of solids.[3]

In contrast, at the high intensity irradiation (high-I) regime, with photon energy either above or below the bandgap, thermal ablation of the semiconductor takes place producing extensive surface modifications as a result of mass loss in the form of ionized and neutral species: atoms, molecules and small clusters.[4] Surface structuring observed in the ablation regime is generally related to the backscattering of the ejected products in collisions with the surrounding atmosphere.[5]

It is noteworthy that considerably less attention has been directed to studies of semiconductor surface modifications induced by irradiation at the intermediate-I regime, which produces high density of electronic excitation in the solid but leads to deposited energy that is well below the thermal ablation threshold. In this case surface modifications may appear as a result of local expulsion of neutrals and excited species at the nanoscale because of electronic energy transfer from excitons or electron-hole plasma (EHP). The critical excitation density of the bulk solids can be compared to the Mott density, which corresponds to the semiconductor-metal transition.[6] Above the Mott density, excitons lose their individual character, resulting in EHP formation.

A relevant effect in bulk solids, which has received much attention during recent years, is the so-called "cold melting"[7–9] observed upon irradiation of solids with ultrashort laser pulses and studied by means of time-resolved reflectivity and x-ray diffraction measurements. A nonclassical mechanism has been proposed, in order to explain "cold melting" that involves solid matrix destabilisation via a transfer of approximately 15% of bound valence-band (VB) electrons to the conduction band (CB).[10] Such an extensive electronic excitation can take place by use of

a)Author to whom correspondence should be addressed. Electronic mail: andrei.kanaev@lspm.cnrs.fr.

excitation pulses with durations shorter than the characteristic time of electron-phonon relaxation: $\tau_L \leq \tau_{e\text{-}ph} \approx 1\text{–}10$ ps.

In this context, processes involving high density electronic excitation of semiconductors appear quite interesting both in terms of understanding a number of fundamental phenomena, for example, electronically induced nonequilibrium phase transitions and in terms of exploring new technological regimes for materials processing or photonic applications.[11]

Recently, Shih *et al.*[12] have reported on the fast dielectric function analysis of mono-crystalline ZnO that was found to be strongly perturbed by a high charge-carrier density. Employing femtosecond pulses from a Ti:sapphire laser (800 nm) with energy density 240 mJ/cm^2, slightly below the ablation threshold (300 mJ/cm^2) they observed interesting features related to charge and exciton relaxation mechanisms. No systematic observations concerning crystal surface structure, following irradiation in this regime, were reported, while ripples were observed for irradiation above the ablation threshold. Considering that the bandgap energy for ZnO is much higher than the photon energy employed, it is understood that the density of electronic excitation achieved in these experiments was rather limited because of a low-probability inherent to multiphoton transitions; absorption by impurities and structural defects in these conditions results in thermal ablation. Clearly, a higher electronic excitation density regime can be better attained through a direct interband excitation of ZnO with UV photons at $\lambda \leq 360$ nm.

Using direct interband excitation of a femtosecond KrF laser (248 nm; 450 fs), we have recently observed a giant photoluminescence (PL) enhancement upon irradiation of monocrystalline ZnO samples. This PL enhancement correlates with the surface roughness modifications which were found to appear even at irradiation energy density (fluence) values being as much as 10 times lower than the ablation threshold fluence ($E_a = 115$ mJ/cm^2).[13] Although PL emission is often sample-dependent (because of the different trace impurities profile in differently prepared crystals), the enhancement of photoluminescence, produced upon ultrafast irradiation of ZnO crystals, can serve as a sensitive probe of the induced surface micro- and nano-structuring. We have addressed the macroscopic response of irradiated ZnO samples, while the microscopic picture of the effect was beyond the scope of those studies.

In this communication, we show that irradiation of ZnO leading to high-density electronic excitation, above the Mott density but well below the ablation and even melting thresholds, can strongly affect the surface and bulk morphology of the crystalline samples. We show a correlation of PL emission with the extent of the observed surface nanostructuring, which has a characteristic unit size much below the diffraction limit ($1/25\lambda$). Notably, the observed effects are reproducible for different ZnO samples and seem to be of universal character for semiconductor solids.

II. EXPERIMENT

Laser experiments were carried out at the Ultraviolet Laser Facility operating at IESL FORTH (Heraklion, Greece) on a hybrid system comprising a distributed feedback dye laser/KrF excimer laser delivering 450 fs pulses at 248 nm at a repetition rate of 1–10 Hz and energy of 10 mJ spatially distributed across an area of 3 cm^2 × 2 cm^2 (Ref. 14). Monocrystalline ZnO samples with ⟨0001⟩ orientation (tolerance ± 0.5°) and O-terminated were fabricated by a hydrothermal method and supplied by *Semiconductor Wafer Inc*. in pellets 10 mm^3 × 10 mm^3 × 0.5 mm^3 in size with both sides polished (surface roughness 1.0 nm). The laser beam was gently focused onto the sample surface at normal incidence into a circular spot of 1 mm or 50 μm diameter. The energy on the sample was varied by using two reflective attenuators and measured using an energy meter. The fluence was carefully calculated taking into account the spot geometry. As a result, the samples were irradiated with fluence in the range of 0.3 to 150 mJ/cm^2 under ambient atmosphere and at room temperature. The number of irradiation pulses was 1–10^4 in the present experimental series.

Besides single laser pulse irradiation experiments, a series of double-pulse measurements was carried out, termed "pump-pump" experiments in order to clarify the energy threshold for surface modification. By use of a Michelson-type interferometer, the original laser beam was split into two beams of equal intensity, which were collinearly superimposed on the sample surface. A time delay between the two laser pulses of 0–1000 ps was introduced by translating one interferometer arm.

Irradiation experiments were performed in two modes: with large beam opening and with spatial beam selection. Using the large beam opening mode permits irradiation of a larger sample area (diameter 1 mm) suitable for *ex situ* bulk characterizations: PL measurements, x-ray diffraction, etc. In contrast, the fine surface analysis by emission scanning electron microscopy (FESEM) was performed on a much smaller area of the sample, approximately 50 μm in diameter irradiated using the spatial beam selection mode. This permits accurate laser fluence control at the expense of energy and, hence, modified ZnO mass. The beam profiles corresponding to the two irradiation modes are shown in Fig. 1.

The focused beam homogeneity was monitored on a UV-CCD camera (Fig. 1). The spatial distribution of the energy in the 1 mm laser spot was reproducible consisting of a relatively smooth plateau with several local maxima of average diameter around 50–100 μm and energy at 60% or higher relative to the mean intensity measured across the whole laser spot. Additionally the uncertainty related to the pulse-to-pulse laser energy fluctuations was estimated to be approximately 20%. Summing up, in experiments performed at the large beam opening mode, the absolute fluence error bar at approximately 80% was estimated as the sum of local and temporal fluctuations. For experiments performed at the spatial beam selection mode, a small part of the laser beam filtered by an iris diaphragm was focused on the sample: the energy distribution over the irradiated spot of ~50 μm diameter was having a smooth Gaussian shape with no spikes. The laser fluence definition in this mode was only related to the pulse-to-pulse laser energy fluctuations being about 20%.

The level of sample excitation was controlled through the PL spectra intensity. The photoluminescence was

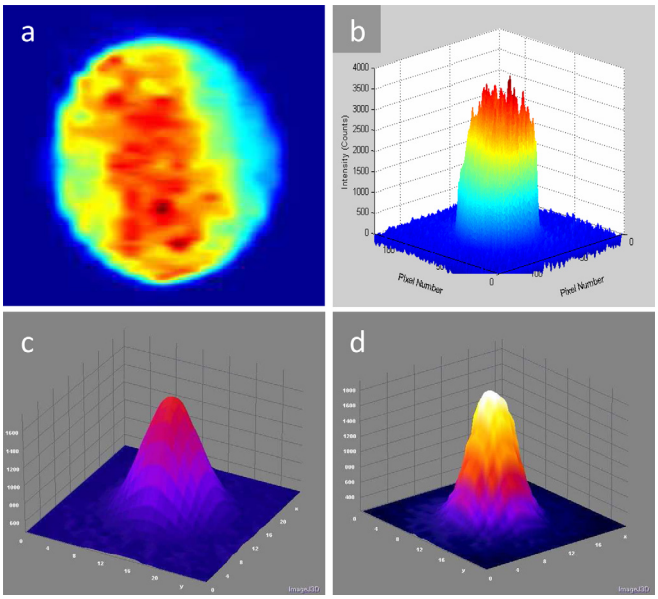

FIG. 1. (Color online) Spatial profile of the KrF laser beam (single shot) on the sample in two irradiation regimes (a and b) with large beam opening and (c) with spatial beam selection of one beam and (d) of two superimposed beams. The spot diameters are (a and b) ~1 mm and (c and d) ~50 μm (full width half maximum), respectively.

collected by a quartz lens and focused on a multimode quartz optical fiber. A compact spectrograph (TRIAX-320, Horiba Jobin-Yvon) equipped with a concave holographic grating (600 grooves/mm), combined with an ICCD detector (DH520-18 F, Andor Technology) was used to record the time-integrated emission spectrum from 200 to 800 nm with a resolution of about 0.4 nm. A picosecond-resolution streak camera (C5680 series by Hamamatsu Photonics) was used for PL lifetime measurements.

Low temperature PL spectra were measured *ex situ* at SUPERLUMI experimental station of HASYLAB (synchrotron DESY, Hamburg).[15] Briefly, samples were cooled down to 8 K and irradiated by monochromatized synchrotron radiation (SR) with $\Delta\lambda = 3.3$ Å under high vacuum ($\sim 10^{-9}$ mbar). The measurements of luminescence spectra were carried out using a visible 0.275-m triple-grating ARC monochromator equipped with a CCD detector or a photomultiplier operating in the photon- counting mode. The pulse structure of SR (130 ps, 5 MHz repetition rate) enables time-resolved luminescence analysis at time-scale of 200 ns with sub-nanosecond temporal resolution and corrected for the primary monochromator reflectivity and SR current. Spectra can be recorded within a time gate $\Delta\tau$ delayed after the SR excitation pulse. Typically two time gates have been used simultaneously: a fast one of $\Delta\tau_1 = 2 - 8$ ns and a slow one of $\Delta\tau_3 = 50 - 200$ ns.

The samples were structurally characterized by using x-ray diffraction (XRD) installation INEL XRG 3000 with CuKα radiation with Nickel filter.

The surface morphology was examined on a Jeol Scanning Microscope JSM 7000 F, which employs a Schottky type field-emission (T-FE) gun for the electron source operating at pressure 10^{-8} Pa, with a function for high-resolution image observation. The spatial resolution achieved is 1.2 nm at 30 kV (max accelerating voltage).

III. RESULTS AND DISCUSSION

A. Nanostructuring of monocrystalline ZnO

The characteristic UV photoluminescence emission of ZnO is employed as an indirect probe to determine the nature and the extent of electronic excitation. For this reason, room-temperature luminescence spectra of the ZnO monocrystal were collected for different values of excitation fluence following excitation with 450 fs laser pulses at 248 nm (Fig. 2). The low-density excitation regime was realized at fluence values $E \leq 0.3$ mJ/cm^2 giving rise to exciton luminescence emission with a spectral maximum at 379 nm (Fig. 2, curve a). As excitation density increases, more and more electron-hole pairs are created within the excitation volume. In fact, since both the exciton and the EHP lifetimes are long compared to the laser pulse duration (450 fs), their instantaneous number density $n_{e\text{-}h}$ can be considered as proportional to the laser fluence. When $n_{e\text{-}h}$ increases above the Mott density, excitons are no longer a stable elementary excitation and the electron-hole plasma is produced. The critical Mott density of ZnO crystals n_{Mott} can be evaluated according to:

$$n_{Mott} = \frac{k_B T}{2a_B^3 E_B} \approx 4 \times 10^{19}\ \mathrm{cm}^{-3}, \qquad (1)$$

where k_B is the Boltzmann constant, T is temperature and E_B =60 meV and $a_B = 1.8$ nm are, respectively, the exciton binding energy and Bohr radius.[16,17] The EHP luminescence continuum is broad and has its emission maximum at about 400 nm. It shows up in the measured spectra (Fig. 2, curve b) as the long-wave shoulder of the principal exciton band.

The growth of the EHP is shown in Fig. 3, where the integral intensity of the EHP continuum is plotted as a function of the laser fluence. The EHP band appears at fluence values E~0.5 mJ/cm^2 and continues growing for E up to ~4 mJ/cm^2. This result clearly demonstrates the onset of the EHP regime at E_{EHP}=0.4 ± 0.1 mJ/cm^2. Taking into account the intrinsic material absorption, this value corresponds to the instantaneous density of photoinduced charges n_{Mott} from Eq. (1). We therefore assign the threshold fluence E_{EHP} to the Mott transition. Above the Mott density, the exciton PL intensity is no longer linearly dependent on laser fluence reaching saturation at $E \geq 4$ mJ/cm^2. This is a strong indication that non-radiative

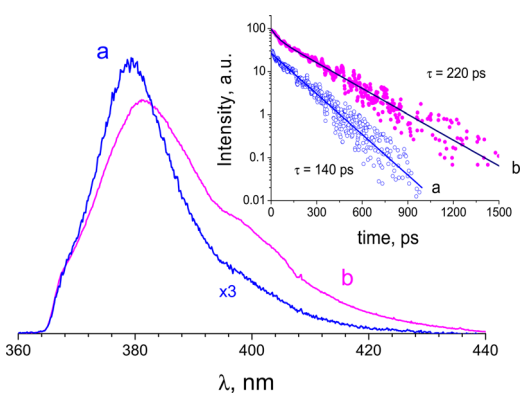

FIG. 2. (Color online) Room temperature PL emission spectra of 0001 ZnO monocrystal at fluences (a) 0.3 mJ/cm^2 and (b) 3 mJ/cm^2. Inset: PL emission decay at fluences (a) E_L=1 mJ/cm^2 and (b) 18 mJ/cm^2.

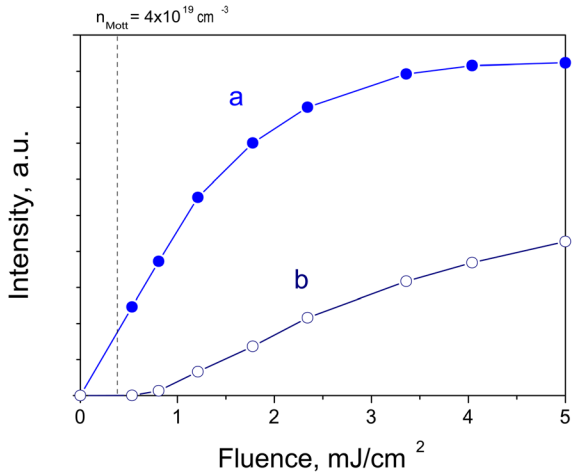

FIG. 3. (Color online) Intensity of the 0001 ZnO monocrystal exciton (a) PL and (b) EHP emissions as a function of laser fluence (248 nm, 450 fs). The vertical dashed line indicates the onset of the EHP emission continuum.

processes involving exciton quenching become dominant in these conditions.

The PL decay of EHP shows a major component with lifetime 140 ps at low irradiation fluences (Fig. 2, curve a in inset). However, under highly saturating conditions (E = 18 mJ/cm^2) it becomes somewhat longer $\tau \approx 220$ ps (Fig. 2, curve b in inset).

Upon exposure of the monocrystalline ZnO sample to the UV femtosecond pulses structural modifications were observed as shown in Fig. 4 that could be correlated with the irradiation fluence. In fact three types of structuring can be evidenced. (1) At fluence levels below 11 mJ/cm^2 rare volcano-like nanoholes, randomly distributed across the sample surface, were observed [Fig. 4(a)] having a diameter of $D_1 \approx 60$ nm and showing clear melt-like features around their rims. With prolonged irradiation, the initial D_1-holes disappear while new ones appear of the same size. The D_1-holes formation process terminates at high doses giving rise to just flat featureless surfaces. (2) At higher fluence

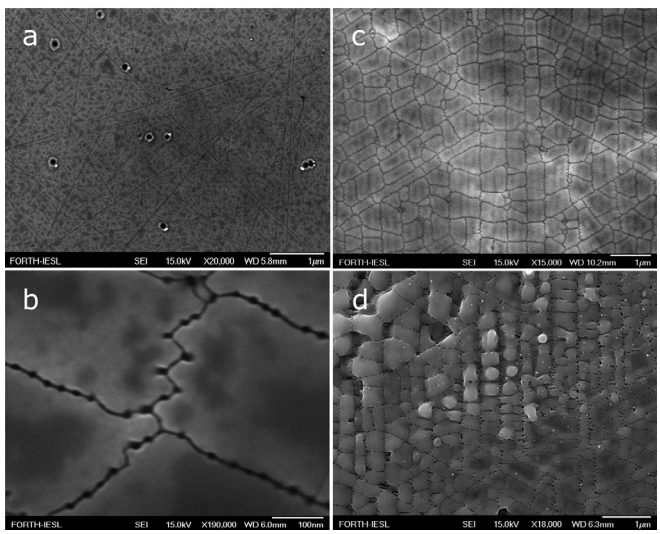

FIG. 4. FESEM images of the irradiated 0001 ZnO monocrystal (248 nm, 450 fs) at fluences (a) 10 mJ/cm^2, (b and c) 20 mJ/cm^2, and (d) 40 mJ/cm^2; corresponding irradiation dose is (a) 2.5 J/cm^2 and (b–d) 10^2 J/cm^2.

levels, but below 40 mJ/cm^2, extensive nanostructuring appears all across the sample surface [Fig. 4(b) and 4(c)]. The smaller nanoholes of $D_2 \approx 10$ nm diameter appear quasi-periodically separated by a distance of approximately 30 nm. They are aligned either along straight or zigzag-type lines. As a result, the monocrystalline surface breaks down to domains of size $\sim 10^2$ nm surrounded by the interconnected D_2-nanoholes. The contrast of this remarkable pattern initially improves with irradiation time. The structure stabilizes at irradiation doses above ~ 1 J/cm^2; no more changes were observed in the dose range between 1 and 10^2 J/cm^2. (3) At laser fluences above 40 mJ/cm^2 the nanostructuring pattern of regime (2) remains, however the surface becomes unstable [Fig. 4(d)]. Swelling, detachment of small nanolayers and formation of metal (Zn) nanoparticles can be observed.

We remark that the laser fluence levels corresponding to regimes (1)–(3) are well below the ablation threshold measured to be E_a=115 mJ/cm^2. The critical laser fluence E_{12} separating regimes (1) and (2) corresponds to the threshold of the PL emission enhancement E*=11 mJ/cm^2 reported by Museur *et al.*[13] Moreover, the critical laser fluence E_{23}=40 mJ/cm^2 separating regimes (2) and (3) corresponds to the beginning of the surface melting: $E_{23} \approx E_m$. Indeed, this fluence can be estimated on the basis of known properties of ZnO: specific heat $c_p = 0.40$ J/gK, mass density $\rho = 5.7$ g/cm^3, melting temperature $T_m = 2275$ K and optical penetration depth $\delta \approx 100$ nm at 248 nm. Neglecting material thermal conductivity, one obtains the melting threshold fluence as: $E_m = c_p \rho \delta \Delta T \approx 45$ mJ/cm^2 (with $\Delta T = T_m - T_{\text{room}} = 1982$ K).

The PL emission enhancement has been confirmed in our monocrystalline samples irradiated at fluence values above E_{12}. An example of the low-temperature PL spectra before and after irradiation is shown in Fig. 5. The analyzed ZnO sample was laser irradiated at 16 regularly spaced spots of ~ 1 mm diameter. The mean fluence was maintained at ~ 24 mJ/cm^2. This value bears an uncertainty of about $\pm$ 19 mJ/cm^2 (80%) that reflects the spatial and temporal inhomogeneities of the laser beam, as detailed in the experimental section. Therefore, we can assign the related structuring mainly to regime (2), however, the surface erosion characteristic of regime (3) is attributed to irradiation at fluence levels corresponding to the positive extremes of the beam energy fluctuations. The integrated PL from the modified surfaces is found enhanced 10 times relative to that of the unexposed crystal. Moreover, the PL spectral shape changes becoming more symmetric as a result of an apparent low-energy tail extension.

The PL emission line shape of the fresh ZnO monocrystal, with a full width at half maximum (FWHM) of about 6 meV, is defined by the A excitons bound to neutral donors (DBE): $D^0{}_1X_A$ at 3.3598 eV, $D^0{}_2X_A$ at 3.3605 eV, $D^0{}_3X_A$ at 3.3618 eV, $D^0{}_4X_A$ at 3.3650 eV and $D^0{}_5X_A$ at 3.3664 eV with $D^0{}_2X_A$ being the most intense, which is in agreement with Teke *et al.*[18] The low-energy tail of PL is formed by transitions previously assigned to the acceptor-bound excitons (ABE): stronger $A^0{}_1X_A$ at 3.3564 eV and weaker $A^0{}_2X_A$ at 3.3530 eV and $A^0{}_3X_A$ at 3.3481 eV (see review in Ref. 16). These ABE transitions seem to intensify after laser irradiation of the monocrystal. In contrast, two-electron satellite

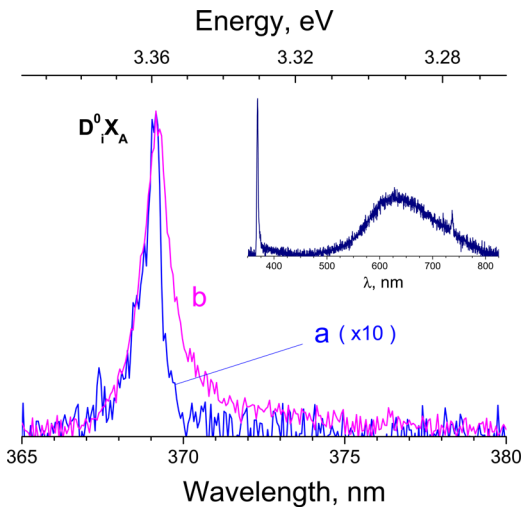

FIG. 5. (Color online) Low temperature (8 K) UV PL emission spectra of the (a) fresh and(b) irradiated 0001 ZnO monocrystal (sample irradiation: 248 nm, 450 fs, fluence 24 ± 12 mJ/cm^2, mean dose 360 J/cm^2). The intensity of spectrum (a) is multiplied by a factor of 10. Inset: full UV-visible emission spectrum of the irradiated sample.

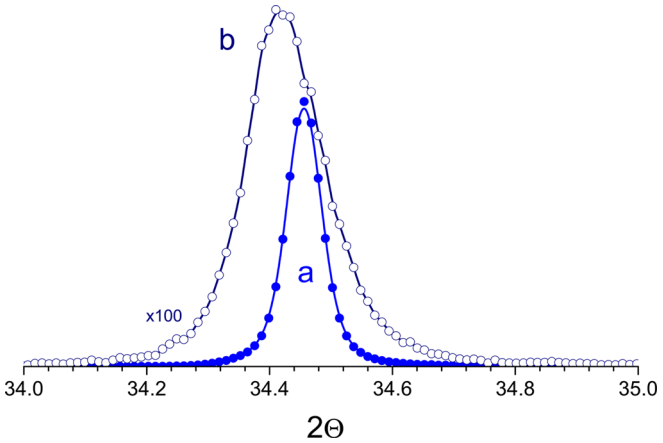

FIG. 6. (Color online) XRD pattern of the (a) fresh and (b) irradiated 0001 ZnO monocrystal recorded with the same accumulation time of 38 s (sample irradiation: 248 nm, 450 fs, fluence 24 ± 12 mJ/cm^2, mean dose 360 J/cm^2).

TES transitions in the lower-energy spectral region of 3.32–3.34 eV were not observed. The chemical origin of the ABE peaks is not yet understood, however, the $A^0{}_1X_A$ one has been suggested to be due to the presence of Na or Li atoms. Because the impurities content is not expected to increase upon irradiation, the intensified ABE transitions may be related to surface states, whose density increases upon structuring.

The intensification of the exciton PL is accompanied by an intensity decrease of a broad-band red PL at ~1.8 eV by almost 10 times (Fig. 5, inset). This PL is characteristic of non-doped bulk ZnO and has not been yet identified.[16] We remark that the green luminescence band commonly observed in both non-doped and *n*-type ZnO at 2.5 eV does not show up in the PL emission spectra of our samples. Both oxygen, V_O, and zinc, V_{Zn}, vacancies were previously evidenced as origins of this band. This fact indicates that the monocrystalline ZnO sample does not lose its excellent stoichiometry upon irradiation. As we will see in the following, the photoinduced bond breaking does not lead to isolated vacancies but to nanostructuring.

Results from XRD studies performed on the fresh and irradiated ZnO monocrystal (same sample as the one used in the PL studies (Fig. 5) are shown in Fig. 6. The main 0001 peak of the oriented monocrystalline ZnO is at 2θ=34.456° with Δ_{fwhm}=0.067°. The peak position and linewidth change after irradiation and become respectively 34.418° and 0.147°. Since the characteristic penetration depth of the x-ray is ~100 μm, this indicates profound bulk modification of the irradiated material. The nanostructuring results in a smaller monocrystalline domain of ~0.1 μm size and increases the crystalline interplane c-distance by $\Delta d/d = \Delta\theta/\tan(\theta) = 1.1 \times 10^{-3}$. At the same time, the surface erosion of regime (2) may produce disoriented secondary crystallites at the sample surface, whose diffraction pattern resembles that of ZnO powders. However, the mass of the disoriented matter is extremely low. It is noted that collecting the XRD data from this disoriented matter takes about two days, while the main Bragg bulk reflection 0001 peak shows up after just several seconds.

Apparently, the sample modification in this irradiation regime, $E_{12} \leq E_L \leq E_{23}$ ($E_{12} = 11$ mJ/cm^2 and $E_{23} = 40$ mJ/cm^2) is not related to thermal effects. This was confirmed by the pump-pump experiments. The fluence of each beam was fixed to 9 mJ/cm^2, which (including fluctuations ± 1.8 mJ/cm^2) remains below the nanostructuring threshold energy, E_{12}. On the other hand when the two beams are superimposed, the total fluence falls into regime (2) in which nanostructuring takes place. The delay between the two pulses, Δt, thus evidences the lifetime of the transitory state, which permits the two contributions to be additive. FESEM images of the monocrystal surface following two-pulse irradiation corresponding to different delay times, in the range of 0–500 ps, are shown in Fig. 7. It is quite evident that nanostructuring does not change appreciably for as long as $\Delta t \leq 200$ ps while it gradually reduces and eventually disappears at longer delays. This result suggests the lifetime of a hypothetical excited state responsible for the nanostructuring (NS) to be 200 ps $< \tau_{NS} <$ 250 ps.

Notably, this value τ_{NS} is characteristic of the photoluminescence decay of EHP in our high-quality monocrystalline ZnO at the relevant fluences $E_{12} < E_L < E_{23}$, whose dominant component lifetime is $\tau = 220$ ps (see Fig. 2, curve b of inset). This value is in agreement with PL decay lifetime previously measured on monocrystalline ZnO samples, which vary from 116.5 ps to 170 ps depending on whether the fs-laser irradiation fluence was corresponding to excitation below or above the Mott density.[18] A detailed analysis of the PL decay also evidences a very short component with a lifetime of 36 ps. This minor, short-lived component of EHP (~8% energy) corresponds to that reported in measurements performed under similar experimental conditions (300 fs, 273 nm) in monocrystalline (0001) ZnO;[20] it implies a competing thermal cooling of conduction-band electrons and valence-band holes toward the exciton band bottom (renormalized bandgap) through multiple LO-phonon emissions.[17] The samples used in the present experiments exhibit very strong exciton PL (that further improves after irradiation), which is important but seems not to be the major energy

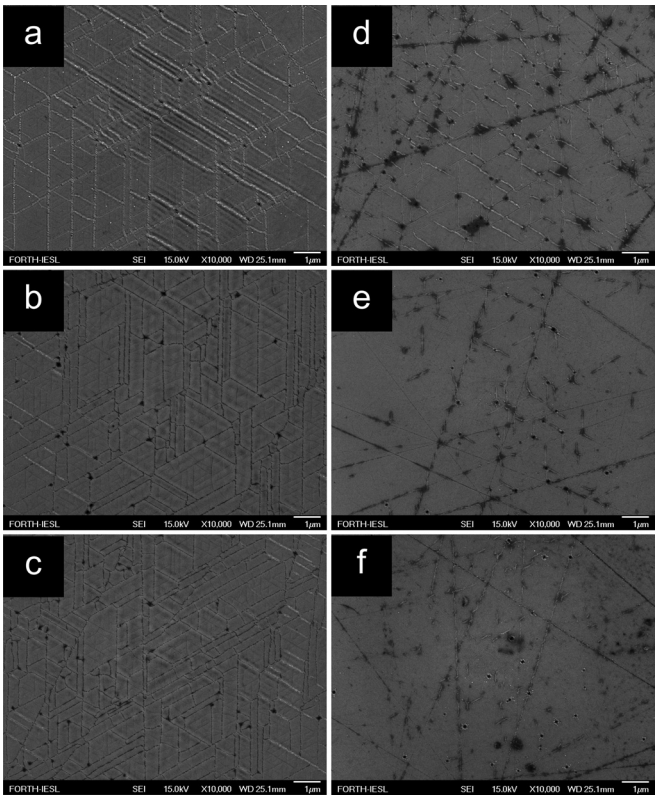

FIG. 7. FESEM images of the 0001 ZnO monocrystal surface irradiated with a pair of pulses at different inter-pulse delays Δt: (a) 0, (b) 100 ps, (c) 200 ps, (d) 300 ps, (e) 400 ps, and (f) 500 ps (sample irradiation: 248 nm, 450 fs, fluence in each pulse 9 mJ/cm^2, dose 18 J/cm^2).

relaxation channel. This is confirmed in recent studies by Ucer *et al.*[19] who have reported 38% quantum efficiency for the D^0X luminescence of in c-axis oriented monocrystalline ZnO samples at low excitation, below the Mott density.

The PL saturation observed with an increase of excitation fluence above the Mott limit (see Fig. 3) proves that most of the photoinduced EHP relaxes through a nonradiative channel. The measured $\tau_{NS} \approx$ 200–250 ps in the pump-pump experiments corresponds to the lifetime of the EHP decay $\tau = 220$ ps. We therefore believe that the measured decay time belongs to a transient state involved in the relevant EHP energy relaxation channel. The high EHP density of $\rho_{eh} \sim 10^{21}$ cm^{-3}, which corresponds to the nanostructuring threshold $E_{12} = 11$ mJ/cm^2, opens an additional energy dissipation channel leading to the nanostructuring.

B. Mechanism of nanostructuring

Possible mechanisms of the PL enhancement have been recently discussed by Museur *et al.*,[13] who concluded that the origin for the enhanced emission was most likely a finest nanostructuring at the scale below 100 nm. Indeed, the relevant nanostructuring is evidenced by the present experiments and its mechanism is discussed in the following.

A correlation between PL improvement and conductivity increase has been reported in monocrystalline ZnO upon laser irradiation.[21,22] This effect has been earlier attributed to the redistribution of point defects, shallow interstitial Zn donors, migrating from decorated dislocations into the crystal bulk. This mechanism, however, does not seem to be appropriate in our case, since n-doped ZnO exhibit strong characteristic green PL, which was not observed in our samples.

It is known that damage in crystals involves energy localization, since the maximum elastic energy per atom which can be stored in a solid before plastic deformation, is considerably lower than that required for bonds breaking.[23] The dislocation density in monocrystalline ZnO grown using a hydrothermal method is expected to be below $\sim 10^6$ cm^{-3} (see Ref. 24). This value can be considerably increased upon irradiation becoming as high as $\sim 10^{10}$ cm^{-2}, which would explain the observed structuring with the mean period of 100 nm. However, it is known that dislocations act as nonradiative recombination centers producing significant quenching of the exciton PL in non-doped ZnO crystals,[25,26] which is not our case.

The observed nanostructuring can be due to cluster vacancies, which accumulate on dislocation sites. The related mechanism of Cottrell atmosphere is well known in materials elasticity theory and explains the residual stress reduction on the basis of interstitials migration to dislocations.[27,28] Accordingly, we propose that point defects migrate toward dislocations following sample irradiation thus producing nucleation and growth of cluster vacancies. This phenomenon may be amplified by the local melt state along these dislocations, which provides to it the threshold character.

In fact, the formation of vacancies by bonds breaking is observed at much lower irradiation fluences and yields.[1,2] The reason of the net acceleration and threshold behavior of the observed phenomenon may be so-called electronic "cold melting," which accompanies the formation of vacancies. This effect can be observed in bulk semiconductors when ~15% of the valence band electrons are transmitted into the conduction band,[7,29] which requires laser fluences close to the ablation threshold. On the other hand, Kwak *et al.* have observed surface disorder of non-thermal nature at much lower excitation level than that needed for global instability.[30] This electronic melting would intensify mass transfer in the surface layer accelerating the nucleation-growth of cluster vacancies. The threshold fluence of nanostructuring 11 mJ/cm^2 indeed corresponds to the excitation ~2.5% of conduction band electrons in ZnO.

A tentative scheme for the structuring mechanism is depicted in Fig. 8. The EHP is created into the ZnO crystal with laser excitation density above the Mott density. The valence-band holes can be localized onto the short-lived (typically subnanosecond[31]) states resulting in bond breaking and surface atoms desorption according to the known two-hole mechanism. This can be observed as a random removal of surface atoms and clustering of vacancies. However, when laser fluence is $E_L \geq E_{12} = 11$ mJ/cm^2, the electronically melt state is reached, which can accelerate transport of vacancies resulting in the observed intense nanostructuring. This melt state, however, is significantly different from the thermally melt state, which induces strong surface deformation and erosion [the beginning of this process is seen in Fig. 4(d)].

The observed surface structuring in the pump-pump experiments can be satisfactorily described by a simple model taking into account vacancies formation and clustering:

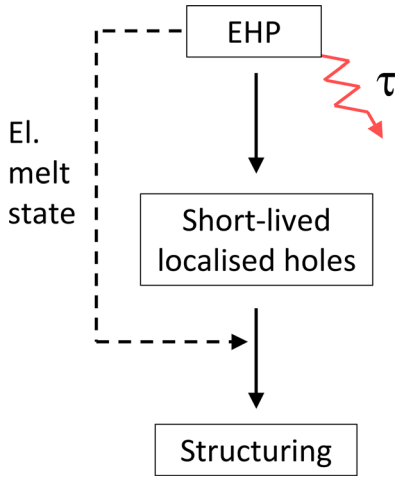

FIG. 8. (Color online) Tentative scheme of the processes and states involved in the nanostructuring mechanism.

$$S \propto N_{vac} \times p_{nucl}, \tag{2}$$

where S is structure density, N_{vac} is vacancies number density, and p_{nucl} is probability of cluster vacancies nucleation. In the pump-pump experiments: $N_{vac} \propto E_{L1} + E_{L2} = 2E_L$ and $p_{nucl} = \tau_{nucl}^{-1}/(\tau_{nucl}^{-1} + \tau_q^{-1})$, where τ_{nucl} and τ_q represent the characteristic nucleation and nucleation quenching lifetimes, respectively. The latter is attributed to the lifetime of a hypothetical transient melt state enabling high mobility of vacancies: $\tau_q = \tau_{melt}$. It can be represented by

$$\tau_{melt} \equiv t_{E_L \geq E_{12}} = \tau \times \ln\left(\left(1 + e^{\Delta t/\tau}\right)E_L/E_{12}\right), \tag{3}$$

where τ is the EHP lifetime, obtained from the luminescence decay in Fig. 2 (inset). The expression describing nanostructuring as a function of the delay Δt between two laser pulses, each with a fluence equal to E_L, is

$$S = kE_L \cdot \frac{\ln\left(\left(1 + e^{\Delta t/\tau}\right)E_L/E_{12}\right)}{\tau_{nucl}/\tau + \ln\left(\left(1 + e^{\Delta t/\tau}\right)E_L/E_{12}\right)}. \tag{4}$$

The dependence of S on Δt for the experimental values of $E_{12}/E_L = 1.3$ and $\tau = 220$ ps is shown in Fig. 9 for different τ_{nucl}. This model explains the absence of structuring in Fig. 7 for $\Delta t > 200$ ps. Moreover since the experimentally observed nanostructuring density is not very different for short delays, $\Delta t \leq 200$ ps (see Fig. 7), it better corresponds to the case $\tau_{nucl} \ll \tau$ in Fig. 9. Thus, it can be concluded that the vacancies nucleation time is of the order of 10 ps or shorter.

We remark that at laser fluence of 20 mJ/cm^2 and irradiation dose of 100 J/cm^2 we observe the surface having 5% of void space in the form of nanoholes [Fig. 4(b) and 4(c)]. This value is typical of the total number of vacancies produced with similar irradiation doses according to the two-hole mechanism.[1,2] However, no acceleration of the structuring kinetics was observed, which implies that the vacancy production is not enhanced by the existing vacancies. Moreover, the nanoholes maintain their size while their density saturates at long irradiation times. The nanostructured surface may therefore be more stable against defect creation than the initial one.

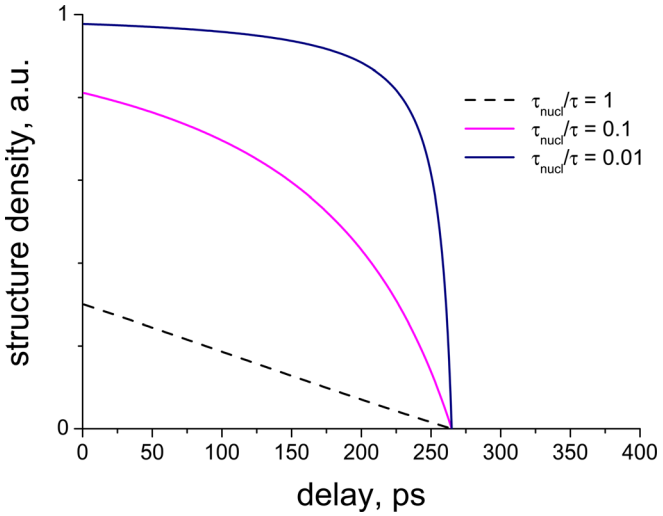

FIG. 9. (Color online) Surface structure density vs inter-pulse delay Δt in pump-pump experiments, according to Eq. (4) ($E^*/E_L = 1.3$, τ =220 ps).

In support of the proposed mechanism, we refer to the size-dependent pore formation in GaSb nanoparticles that has been recently observed.[32] The suggested mechanism involves vacancies cluster growth forming a void whereas surface segregation of interstitials causes a two-phases separation. According to that work, void formation can only be observed in particles larger than 10 nm. The underlying mechanism seems to be similar to that in the present experiments. Unlike GaSb, oxygen in ZnO can form gaseous molecules, which escape from the sample. The remaining element, Zn, is subjected to aggregation leading to formation of Zn-nanoparticles at prolonged irradiation; the beginning of this process can be observed in Fig. 4(d). It is noted that a complete surface coverage by Zn-nanoparticles was observed at higher fluences and irradiation doses above 300 J/cm^2.

We remark that the majority of dislocations in monocrystals are formed close to the surface and their density in the nearest 100-μm layer beneath the surface can be considerably higher than that in the bulk. Since dislocations serve as nucleation sites for vacancies, it is not surprising that nanostructuring begins at the sample surface. The issue of the vacancies mobility in the melt layer and the reason of their quasi-periodic clustering remain unclear.

As a result of the nanostructuring, the density of dislocations may decrease, which leads to an increase of the exciton PL efficiency, in agreement with our experimental results. In parallel the decrease of the red PL band intensity allow us to assume that this band can be dislocation-related.

IV. CONCLUSION

We report on surface modifications of monocrystalline wurtzite (0001) ZnO excited by femtosecond laser pulses (248 nm) above the Mott density (E_{Mott}~0.4 mJ/cm^2) but well below the ablation threshold fluence (E_a=115 mJ/cm^2). Three types of structuring can be evidenced based on the laser fluence, E_L, defining three irradiation regimes. (1) At

fluence levels $E_{Mott} < E_L < E^* = 11\ \mathrm{mJ/cm^2}$ rare volcano-like nanoholes form randomly across the sample surface having a diameter of $D_1 \approx 60$-nm and a clear melt-shape crater rim. We assign the formation of this type of nanoholes to deep impurity explosion by multiple excitons condensation. (2) At fluence levels $E^* < E_L < E_{melt} = 40\ \mathrm{mJ/cm^2}$ extensive nanostructuring appears all across the sample surface. Nanoholes with a diameter of 10 nm and inter-hole distance $\sim$30 nm are arranged along straight and zigzag-type lines. This nanostructuring results in the formation of smaller monocrystalline domains of $\sim 10^2$ nm and increases the crystalline interplane c-distance by 0.11%. The excitonic PL of the irradiated sample is found to increase by about 10 times. We tentatively assign the observed structuring to the nucleation-growth of cluster vacancies at dislocations accelerated by the non-thermal (electronic) melting of the surface layer, which provides threshold character to this phenomenon. On the basis of dual pulse irradiation (pump-pump experiments) the melt state lifetime is estimated to be quite similar to the EHP lifetime ($\tau = 220$ ps). A simple model is presented permitting a conclusion about the short nucleation time of the photoinduced vacancies in the melt state, $\tau_{nucl} \ll \tau$. (3) At laser fluence levels $E_{melt} < E_L$ the surface becomes unstable and subjects to swelling, detachment of small nanolayers and formation of zinc nanoparticles.

ACKNOWLEDGMENTS

This work was carried out in part at the Ultraviolet Laser Facility operating at IESL-FORTH with support from the access activities of the EC FP7-Infrastructures-2007 project "Laserlab-Europe II" (Grant Agreement No. 228334). The PL studies have been carried out at HASYLAB-DESY within the project II-20080156 EC of the EU contract ELISA-226716. The authors are indebted to *Apostolis Egglezis* for invaluable technical support.

[1]N. Itoh and A. M. Stoneham, J. Phys.: Condens. Matter **13**, R489 (2001).
[2]K. Tanimura and J. Kanasaki, J. Phys. Condens. Matter **18**, S1479 (2006).
[3]M. Runne and G. Zimmerer, Nucl. Instr. Meth. B **101**, 156 (1995).
[4]D. Bäuerle, *Laser Processing and Chemistry* (Springer, Berlin, 2000).
[5]S. Klose, E. Arenholz, J. Heitz, and D. Bäuerle, Appl. Phys. A: Mater. Sci. Process. **69**, S487 (1999).
[6]N. F. Mott, *Metal-Insulator Transitions* (Taylor and Francis, London, 1974).
[7]S. K. Sundaram and E. Masur, Nature Mater. **1**, 217 (2002).
[8]C. W. Siders, A. Cavalleri, K. Sokolowski-Tinten, C. Toth, T. Guo, M. Kammler, M. H. von Hoegen, K. R. Wilson, D. von der Linde, and C. P. J. Barty, Science **286**, 1340 (1999).
[9]A. Rousse, C. Rischel, S. Fourmaux, I. Uschmann, S. Sebban, G. Grillon, P. Balcou, E. Förster, J. P. Geindre, P. Audebert, J. C. Gauthier, and D. Hulin, Nature **410**, 65 (2001).
[10]J. S. Graves and R. E. Allen, Phys. Rev. B **58**, 13627 (1999).
[11]J. Dai, C. X. Xu, P. Wu, J. Y. Guo, Z. H. Li, and Z. L. Shi, Appl. Phys. Lett. **97**, 011101 (2010).
[12]T. Shih, M. Winkler, T. Voss, and E. Mazur, Appl. Phys. A **96**, 363 (2009).
[13]L. Museur, J.-P. Michel, P. Portes, A. Egglezis, A. Stassinopoulos, D. Anglos, and A. V. Kanaev, J. Opt. Soc. Am. B **27**, 531 (2010).
[14]S. Szatmári and F.P. Schäfer, Opt. Commun. **68**, 196 (1988).
[15]G. Zimmerer, Nucl. Instr. Meth. A **308**, 178 (1991).
[16]Ü. Özgür, Y. I. Alivov, C. Liu, A. Teke, M. A. Reshchikov, S. Doğan, V. Avrutin, S.-J. Cho, and H. Morkoç, J. Appl. Phys. **98**, 041301 (2005).
[17]N. Arai, J. Takeda, H.-J. Ko, and T. Yao, J. Luminescence **119–120**, 346 (2006).
[18]A. Teke, Ü. Özgür, S. Doğan, X. Gu, H. Morkoç, B. Nemeth, J. Nause, and H. O. Everitt, Phys. Rev. B **70**, 195207 (2004).
[19]K. B. Ucer, R. A. Wall, K. C. Lipke, and R. T. Williams, Phys. Status Solidi B **245**, 2680 (2009).
[20]G. Xiong, J. Wilkinson, K. B. Ucer, and R. T. Williams, J. Phys.: Condens. Matter **17**, 7287 (2005).
[21]I. V. Markevich, V. I. Kushnirenko, A. Baidullaeva, B. M. Bulakh, and P. V. Pobirovskiy, Semicond. Phys. Quantum Electron. Optoelectron. **7**, 350 (2004).
[22]I. V. Markevich, V. I. Kushnirenko, L. V. Borkovska, and B. M. Bulakh, Phys. Status Solidi C **3**, 942 (2006).
[23]K. L. Tsang, Y. Chen, and H. T. Tohver, Phys. Rev. B **30**, 6093 (1984).
[24]G. Dhanaraj, M. Dudley, D. Bliss, M. Callahan, and M. Harris, J. Cryst. Growth **297**, 74 (2006).
[25]I. V. Markevich, V. I. Kushnirenko, L. V. Borkovska, B. M. Bulakh, and A. V. Rusavsky, Phys. Status Solidi C **4**, 3086 (2007).
[26]K. Yoshino, M. Yoneta, and I. Yonenaga, J. Mater. Sci.: Mater. Electron. **19**, 199 (2008).
[27]A. Cottrell and B. Bilby, Proc. Phys. Soc. London A **62**, 49 (1949).
[28]D. Blavette, E. Cadel, A. Fraczkiewicz, and A. Menand, Science **17**, 2317 (1999).
[29]P. Stampfli and K. H. Bennemann, Appl. Phys. A **60**, 191 (1995).
[30]H. Kwak, K. C. Chou, J. Guo, and H. W. K. Tom, Phys. Rev. Let. **83**, 3745 (1999).
[31]J. Kanasaki and K. Tanimura, Phys. Rev. B **66**, 125320 (2002).
[32]H. Yasuda, A. Tanaka, K. Matsumoto, N. Nitta, and H. Mori, Phys. Rev. Lett. **100**, 105506 (2008).